Lab on a Chip

PAPER

View Article Online
View Journal

Cite this: DOI: 10.1039/c9lc01024f

All-in-one platform for salivary cotinine detection integrated with a microfluidic channel and an electrochemical biosensor†

Kyungyeon Lee, ‡[a] Taehee Yoon, ‡[a] Hee-seon Yang, [b] Sunyeong Cha, [b] Yong-Pil Cheon, [b] Leila Kashefi-Kheyrabadi §*[a] and Hyo-Il Jung *[a]

Medical disorders caused by second-hand smoke are a major public health concern worldwide. To estimate the level of second-hand smoke exposure, salivary diagnostics for cotinine analysis is a compelling alternative in conventional diagnostics using bio-fluids, such as blood and urine, owing to its simple and non-invasive collection method. However, there are several critical issues, such as tedious multisteps, demand for expertise, and field unavailability to collect and transport the purified saliva for further analysis. Here, an all-in-one platform is presented to simply collect real human saliva and directly deliver it onto the biosensing surface. The platform consists of a commercial cotton-swab-type collector, 3D-printed housing, and microfluidic channel integrated with an electrochemical competitive immunosensor to evaluate the level of salivary cotinine. The immunosensor is based on a competitive binding assay between cotinine-conjugated horseradish peroxidase (C-HRP) and cotinine for anti-cotinine binding sites. The current responses obtained from the HRP–thionine–H_2O_2 system decreased proportionally to the cotinine concentration. This immunosensor successfully detected its target over a range of 1×10^{-1} to 1×10^{4} pg ml^{-1} with a low limit of detection of 6×10^{-2} pg ml^{-1} and a limit of quantification of 1×10^{-1} pg ml^{-1}. In addition, the platform is applicable to various commercial cotton-swab-type saliva collectors and can successfully transfer the saliva in wide flow rates ranging from 0.1 to 30 ml min^{-1} without leakage or damage to the sensing surface. Furthermore, the practicality of the proposed platform was evaluated by measuring cotinine in real human saliva from eight non-smokers. The concentration of cotinine was from 45.7 to 890.8 pg ml^{-1}, which was in good agreement with that measured by liquid chromatography-tandem mass spectrometry (LC-MS/MS). The introduced all-in-one platform represented a reliable performance delivering simple and practical steps in salivary diagnostics.

Received 15th October 2019,
Accepted 2nd December 2019

DOI: 10.1039/c9lc01024f

rsc.li/loc

1. Introduction

Second-hand smoke refers to the exposure to tobacco smoke in all areas where it occurs (home, workplaces, public places, *etc.*). It consists of 15% of mainstream smoke from smokers' exhalation and 85% of sidestream smoke from the burning tobacco tip. Sidestream smoke contains more carcinogens than mainstream smoke.[1,2] Owing to the effect of sidestream smoke, even a short exposure to second-hand smoke can be harmful to one's health. Second-hand smoke is associated with several diseases, including lung cancer, heart disease, stroke, and sudden infant death syndrome, and causes more than 1.2 million deaths each year.[3] To reduce smoking-related illnesses and deaths, the World Health Organization (WHO) enacted the Framework Convention on Tobacco Control (FCTC), and 181 countries participated. In many countries (South Korea, USA, EU, India, *etc.*), smoking in public places has been prohibited. However, owing to varying degrees of implementation, non-smokers are still vulnerable to the effects of second-hand smoke.[4]

Nicotine, an alkaloid found in tobacco, is predominantly metabolized to cotinine.[5] Cotinine is generally considered an ideal biomarker to monitor tobacco exposure as it has a longer half-life (~20 h) than nicotine (~2 h) and is detectable up to several days after exposure to tobacco.[6] Exposure to tobacco smoke in both actively and passively exposed individuals can be monitored by measuring the cotinine in various biological fluids.[7–9] The salivary cotinine concentration in

[a] Department of Mechanical Engineering, Yonsei University, Seoul 03722, Republic of Korea. E-mail: leila@cau.ac.kr, uridle7@yonsei.ac.kr
[b] School of Biological Sciences and Chemistry, Sungshin Women's University, Seoul 02844, Republic of Korea

† Electronic supplementary information (ESI) available. See DOI: 10.1039/c9lc01024f

‡ These authors contributed equally to this work.

§ Present address: Department of Integrative Engineering, Chung-Ang University, Heukseok-dong, Dongjak-gu, Seoul 06910, Republic of Korea.

non-smokers exposed to second-hand smoke has been reported as 0.04–14.9 × 10^3 pg ml^{-1}, and 13–653 × 10^3 pg ml^{-1} of salivary cotinine was reported for smokers.[10] Saliva has recently attracted much attention for monitoring different biomarkers in the human body thanks to non-invasive and simple methods of collection.[11] In addition, salivary diagnostics showed high sensitivity and a good correlation level compared with blood-based *in vitro* diagnostics.[12–14]

One of the representative methods in conventional saliva collection is the spitting method. This method has the advantage of a simple collection without the need for experienced experts. However, the saliva collected by the spitting method is difficult to implement directly onto biosensors due to the presence of bubbles and debris.[15,16] Therefore, in order to use the saliva for a biosensor, multiple and tedious steps need to be carried out, as shown in Fig. 1A.[17,18] The collected saliva should be centrifuged to obtain pure saliva without debris, and then only the separated supernatant is placed onto the biosensor surface using a quantitative tool such as a pipette. This approach has to rely on laboratory equipment, which makes it challenging to implement for on-site diagnosis.

In this regard, an all-in-one platform is introduced that consists of a cotton-swab-type saliva collector, 3D-printed housing, fixed-volume microfluidic chip, and a competitive electrochemical immunosensor for the detection of cotinine (Fig. 1B). The cotton-swab-type collector has the advantages of a low risk of sample contamination, easy extraction of the pure saliva sample, and usability for babies and physically disabled people.[19] The saliva obtained by the cotton collector is extracted and delivered through the microfluidic channel. Subsequently, a certain amount of fluid can be confined in a fixed-volume chamber of the microfluidic chip. In this experiment, 7 μl of the volume was fixed. After loading the saliva, the immunosensor is separated from the all-in-one platform and is subjected to a potentiostat to measure the concentration of cotinine.

To the best of our knowledge, no electrochemical immunosensor integrated with a microfluidic chip has been reported to determine salivary cotinine. In the present study, an electrochemical immunosensor based on a competitive binding assay between C-HRP and cotinine for anti-cotinine binding sites is introduced. A competitive-format displacement is carried out based on the affinity difference between cotinine and C-HRP for anti-cotinine binding sites. This replacement was monitored electrochemically by the catalytic activity of HRP in the presence of a thionine–H_2O_2 redox system. In addition, the proposed all-in-one platform based on an electrochemical immunosensor successfully validated the cotinine levels in real human saliva samples and showed good agreement with the LC-MS/MS gold standard method. The platform is applicable to the portable potentiostat and is therefore suitable for point-of-care testing (POCT) for unskilled people. Furthermore, it will help many researchers who are studying salivary diagnostics to proceed in their research.

2. Experimental

2.1. Materials and reagents

Analytical grade thionin acetate (Thi), cotinine, *trans*-4-cotininecarboxylic acid (TCT), nicotine (NIC), *N*-nitrosonornicotine (*NN′*), sodium dihydrogen phosphate, disodium hydrogen phosphate, 1-ethyl-3-(3-(dimethylamino)-

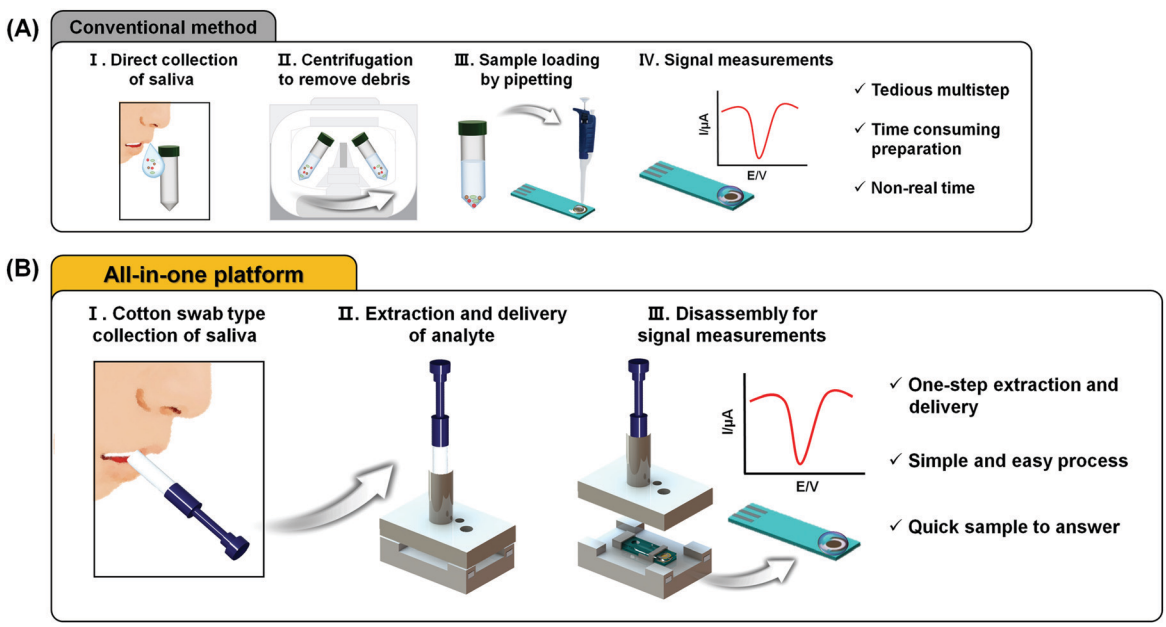

Fig. 1 Schematic illustration of comparison between (A) the conventional method and (B) all-in-one platform for electrochemical based salivary diagnostics.

propyl)carbodiimide hydrochloride (EDC), *N*-hydroxysuccinimide (NHS), sodium chloride, potassium chloride, potassium ferrocyanide, potassium ferricyanide, bovine serum albumin (BSA), and 3-mercaptopropionic acid (MPA) were provided by Sigma-Aldrich. The mouse anti-cotinine and C-HRP were obtained from Creative Diagnostics (DMAB7637) and Fitzgerald (80-1403), respectively.

The anti-cotinine solution was prepared from its stock solution (6.1×10^6 pg ml^{-1}) using phosphate-buffered saline (1× PBS pH 7.4, assay buffer) and stored at −20 °C. The cotinine stock solution was first prepared in absolute ethanol at a concentration of 1×10^{-3} M and kept at 4 °C. The diluted cotinine solutions were freshly made in assay buffer. All solutions were prepared using deionized water (18.2 MΩ cm). Artificial saliva for medical and dental research was acquired from Pickering Laboratories (1700-0305, USA).

2.2. Apparatus

Disposable screen-printed gold electrodes (SPGEs) (DRP-C220BT) were purchased from Dropsens Inc., Spain. Electrochemical experiments were performed using a CHI-650E (CH Instruments, USA) electrochemical analyzer. Electrochemical impedance spectroscopy (EIS) experiments were conducted in an equimolar ferricyanide/ferrocyanide solution (5×10^{-3} M) containing 0.10 M KCl. Nyquist plots were recorded at open circuit (OCP) and an ac potential of 0.005 V over a frequency range of 10 kHz to 0.1 Hz. Cyclic voltammetry (CV) was conducted at a scan rate of 0.1 V s^{-1}. Differential pulse voltammetry (DPV) was applied to quantify cotinine over a range of −0.5 to −0.1 V and recorded at a scan rate of 0.05 V s^{-1} and pulse amplitude of 0.025 V. LC-MS/MS analysis was conducted using an Agilent Technologies 1200 Series LC apparatus coupled with a SCIEX API 4000 LC-MS/MS system (SCIEX, Toronto, Canada).

2.3. Fabrication of all-in-one platform

The fluidic channel and electrochemical biosensor must be connected precisely by a sufficient bonding force and disconnected easily in order to facilitate further analysis. For this reason, the all-in-one platform was divided into four parts: (1) a 3D-printed cover to extract and deliver the saliva sample into the microfluidic channel, (2) a 3D-printed holder to locate the electrode and the microfluidic chip precisely, (3) a microfluidic chip to quantitatively load 7 μl of the saliva sample on the working electrode, and (4) an electrochemical biosensor.

The 3D-printed cover was composed of a saliva extraction part to collect the saliva sample and deliver it into the microfluidic channel, and a jig of 1.5 mm in height (channel-wall shaped) to prevent any leakage between the microfluidic chip and the electrochemical biosensor. The dimensions of the saliva extraction part, 11 (D) × 30 (H) mm (D = diameter, H = height), were determined by taking into account the dimensions of the cotton swabs of three commercially available saliva collectors: Salivette, Super•SAL™, and MiriMoa•SAL Collect. The 3D-printed holder had a grip in the middle, thus fixing the microfluidic chip and the electrochemical biosensor in the correct position. Both the cover and the holder, 60 (L) × 40 (W) × 10 (H) mm (L = length and W = width), were printed in polylactic acid (PLA) using a Sindoh 3D printer, which deposits layers of thermos polymers through a heated extruder. N52 magnets (e-MAGNET, UK) were placed at each corner of the cover and holder so that both parts were connected precisely by the magnetic force. These magnets not only positioned the cover and the holder accurately but also effectively prevented leakage between the electrochemical sensor and the microfluidic chip by pressing the channel wall with magnetic force through the jig designed on the cover part. The 3D printed cover and holder were epoxy treated to avoid any contamination of saliva samples.

Polydimethylsiloxane (PDMS, Dow Corning, USA) as a biocompatible material was utilized to fabricate the microfluidic channel. The channel height was set to 550 μm to quantitatively mount a 7 μl saliva sample on a geometric area of the electrode (12.56 mm^2). The total volume of the microfluidic channel was 30 μl, and the minimum saliva volume for running the assay was equally 30 μl. The organic resin SU-82150 (Microchem Corp., USA) was spin-coated at 500 rpm for 15 s and then at 1250 rpm for 40 s. After a soft baking process for 1 min at 90 °C, the wafer was exposed to ultraviolet (UV) light (450 mJ cm^{-2}) using a photomask that had a channel pattern for 1 minute at room temperature. Then, the item was further baked at 60 °C for 3 min. The SU-8 layer was cleaned with isopropyl alcohol after the layer was developed using an SU-8 developer (SU-8 Developer, MicroChem, Japan). A 10 : 1 volumetric mixture of the PDMS prepolymer and a curing agent (Sylgard 184, Dow Corning, USA) was then poured on the SU-8 mold, followed by degassing in a vacuum chamber. After that, the mixture on the wafer was incubated in an oven at 66 °C for 6 h and then peeled off. Finally, the PDMS was perforated using a punch to create a channel inlet and outlet.

2.4. Preparation of the biosensing surface

Before modifying the electrode surface, the SPGEs were first cleaned using a slightly modified TL1 procedure which was previously described.[20] An aqueous solution containing a 5 : 1 : 1 ratio of $H_2O : NH_3 : H_2O_2$ at room temperature was used for 10 min to clean the working electrode surface.

Then, the electrodes were electrochemically cleaned in 0.5 M H_2SO_4 solution by potential cycling over the range of 0 to 1.1 V until reproducible voltammograms were obtained.[21] The sensing surface was prepared as follows. First, MPA as a linker was self-assembled on a gold electrode surface by placing 7 μl of 50 mM MPA solution on the electrode surface overnight. The MPA-modified electrode was then rinsed, and the carboxylic groups of MPA were activated using an EDC/NHS solution (60 mM and 80 mM, respectively) in 0.1 M PBS (pH 5.0) for 2 h.

First, EDC activates carboxyl groups and forms an amine reactive intermediate. The produced intermediate is unstable

in aqueous solutions. Therefore, NHS is often included in the EDC coupling protocol to improve the efficiency of the reaction. EDC couples NHS to carboxyl groups to form an NHS ester, delivering efficient conjugation to primary amines at physiologic pHs.

After that, the electrode was rinsed again and dried using a N_2 gas stream, followed by placing a 7 μl drop of anti-cotinine (1×10^6 pg ml^{-1}) on the electrode surface for 18 h at 4 °C. To prevent evaporation of the anti-cotinine drop, the electrode was kept in a humid environment. In this step, anti-cotinine was attached to the activated carboxylic groups of MPA through an amide coupling reaction. Then, the unbound antibody was washed with assay buffer and dried using N_2 gas, and 7 μl of 1% BSA solution was put onto the electrode surface for 1 hour to passivate the remaining active sites against non-specific adsorption. Subsequently, after washing and drying the electrode surface, a 7 μl aliquot of C-HRP was dripped on the antibody modified electrode for 0.5 hours to provide the sensing surface for the competitive assay. Finally, the C-HRP/BSA/anti-cotinine/MPA-modified SPGE was rinsed and kept at 4 °C in a humid environment for further use.

2.5. Human saliva samples

Human subjects in these studies were selected in accordance with protocols approved by the Institutional Review Board (SSWUIRB 2017-037) and followed the Declaration of Helsinki (1964).

Saliva was collected in a 15 ml polypropylene tube (Coring, Cat. No. 430791) from eight healthy volunteers without any aid, distributed to 1.5 ml microtubes and stored at −80 °C until analysis using an immunosensor and LC-MS/MS analysis. In addition, the volunteers were asked to complete a questionnaire to observe the status of the exposure to second-hand smoke (Table S1†). For salivary cotinine analysis, the saliva samples were thawed for immediate use with the immunosensor and centrifuged at 5000*g* for 5 min for LC-MS/MS analysis. 100 μl supernatant was taken and mixed with hydroxyapatite (63×10^6 pg ml^{-1}, Sigma) and 400 μl of cold acetone (kept at −20 °C) and then incubated at −20 °C for 16 hours. After incubation, the saliva samples were centrifuged at 20 000*g* for 30 min at 4 °C. The supernatant was transferred into an Agilent kompatible Schraub μ-Vial (glass, 350 μl insert), and 5 μl of the sample was injected into an autosampler for LC-MS/MS.

2.6. Detection of cotinine

A competitive immunoassay was designed to determine the cotinine as follows. First, a 70 μl drop of 0.1 M PBS pH 5.5 (dilution buffer) was dripped on the sensing surface (C-HRP/BSA/anti-cotinine/MPA/SPGE) at ambient room temperature. Then, cyclic and differential pulse voltammograms were recorded. After that, the biosensing surface was rinsed, and a 70 μl drop of dilution buffer containing 0.3 mM Thi was dripped on the sensing surface. Subsequently, cyclic and differential pulse voltammograms were recorded. The sensing surface was washed using PBS solution and DI water. Then, a 70 μl drop of dilution buffer containing 0.3 mM Thi and 2 mM H_2O_2 (probe solution) was placed on the sensing surface and cyclic and differential pulse voltammograms were recorded. During the next step, the sensing surface was washed using PBS solution and DI water and dried and then was incubated with 7 μl of the desired concentration of cotinine antigen for 0.5 hours. Finally, the cotinine/BSA/anti-cotinine/MPA/SPGE was washed with PBS solution and DI water and investigated in probe solution using CV and DPV techniques.

2.7. LC-MS/MS analysis

The LC-MS/MS was equipped with an Agilent Technologies 1200 Series LC apparatus coupled with a SCIEXAPI4000 LC-MS/MS system (SCIEX, Toronto, Canada). Electrospray ionization (ESI) was carried out in the positive ion mode by multiple reaction monitoring (MRM). The following ESI conditions were used: ion spray voltage of 5000 V, source temperature of 500 °C, nitrogen (gas 1) of 50 psi, heater (gas 2) of 50 psi and curtain gas of 20 psi. The decluttering potential (66 V), collision energy (33 V), entrance potential (10 eV), and cell exit potential (6 V) were optimized for cotinine. A quantitative analysis was conducted in MRM with a dwell time of 150 ms. In this study, two different columns were used. The first column was a Security Guard column from Phenomenex (Seoul, Korea), and the second column was an analytical column. An Agilent ZORBAX Eclipse Plus C18 1.8 μm, 3.0 × 10.0 mm (Agilent Technologies) column thermostated at 25 °C was used for the analytical column. Isocratic elution was performed with 5% solvent A (5% ammonium formate in H_2O) and 95% solvent B (methanol) for 5 min at a flow rate of 150 μl ml^{-1}. The MS data acquisition was analyzed using Analyst software (SCIEX, Toronto, Canada). Then, a 5 μl aliquot of the samples was injected into the LC-MS/MS system with an autosampler. Finally, the artificial saliva samples spiked with different concentrations of cotinine from 1 to 1×10^4 pg ml^{-1} and the real human saliva samples collected from eight volunteers were analyzed and quantified.

3. Results and discussion

3.1. Design and operation of the all-in-one-platform

One of our main objectives was to introduce a new concept in which the microfluidic chip can be integrated with an electrochemical sensor, thus allowing for greater functionality of the platform. This concept of stick-and-play is commonly known as a reversible bonding method. Surface attachment using a magnetic force is a typical reversible bonding method. This does not require an additional bonding process such as oxygen plasma bonding and thus reduces the pretreatment steps and fabrication cost. In addition, an assembly driven by magnets can not only ensure an accurate connection between the cover and holder of our platform but

also eliminate the leakage between the microfluidic channel and the electrochemical sensor. For this reason, we implemented a 3D-printed cover and holder with magnets at each corner on the top and bottom, with the microfluidic chip and electrochemical sensor in the middle so they are completely sealed by the magnetic force (Fig. 2A). An image of the all-in-one-platform is shown in Fig. 2B.

Then, we calculated the bonding pressure generated by the magnet. This pressure must be stronger than the pressure of the fluid acting on our microfluidic channel. The strength of the magnets was measured using a gaussmeter (F.W. BELL-5080, Oregon, USA), and the pressure drop (ΔP) of a given velocity was calculated using Hagen–Poiseuille's equation:[22]

$$\Delta P = Q\frac{12\mu L}{wh^3} \quad (1)$$

where ΔP is the pressure drop, μ is the viscosity of the fluid, L is the characteristic linear dimension, w is the width of the channel, h is the height of the channel, and Q is the velocity of the fluid. For our microfluidic chip, μ = 2 mPa s, L = 2 × 10^{-2} m, w = 1500 μm, and h = 550 μm.[25]

In Fig. 2C, a channel outer-wall-shaped jig was designed on the bottom of the 3D-printed cover in order to apply the magnetic force to the outer wall of the PDMS channel, and a grip was fabricated on top of the 3D-printed holder to properly hold the microfluidic chip and electrochemical sensor in the correct position. As a result, the pressure inside the microfluidic channel, set at a flow rate of 30 ml min^{-1}, was 1.92 kPa, and the pressure generated by the magnet inside the platform pushing the channel through the jig was 27.76 kPa. Based on the foregoing numerical calculations, we drew the conclusion that the pressure driven by the fluidic flow inside the channel did not exceed the pressure from the reversible magnetic force.

The operation scheme of the fabricated platform is shown in Fig. 2D. Once the saliva sample in the cotton swab is compressed by the extraction part, the bubble-depleted saliva is injected into the microfluidic channel. Then, the extracted saliva sample fills the confined volume chamber that is on top of the working electrode, and the extra samples move through the outlet once it is completely filled.

3.2. Numerical analysis of the microfluidic chip

The proposed microfluidic chip for the all-in-one platform is shown in Fig. 3A. In order to provide a stable competitive reaction between C-HRP and cotinine for anti-cotinine onto the biosensing surface, the drag force resulting from the fluid flow inside the microfluidic chip should not affect the biosensing surface. However, the drag force increases as the width of the microfluidic channel decreases. Since a high drag force on the biosensing surface has a lethal impact of electrochemical signals on immune complexes, the drag force should be limited within the chip. Indeed, if the applied drag force is stronger than the antigen–antibody interaction force on the biosensor, this will cause breaking of the complexes. It is known that the strength of the antigen–antibody interaction can rupture above 17.5 pN.[23]

For this reason, a numerical analysis using a computer-aided simulation program (COMSOL Multiphysics, USA) was carried out to determine the optimal width of a microfluidic

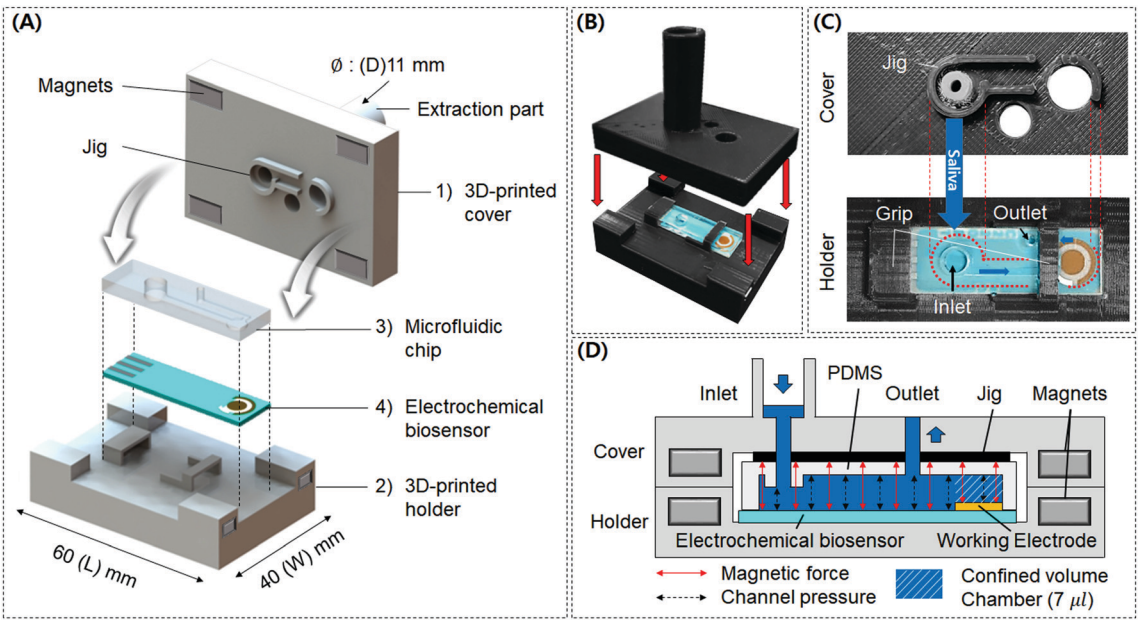

Fig. 2 Design of the all-in-one platform. (A) Configuration and dimensions of the platform modules including the 3D-printed cover and holder, microfluidic chip, and electrochemical biosensor. (B) Real image of the integrated platform. (C) Integration of the microfluidic chip. (D) Side view of the all-in-one platform representing force distribution.

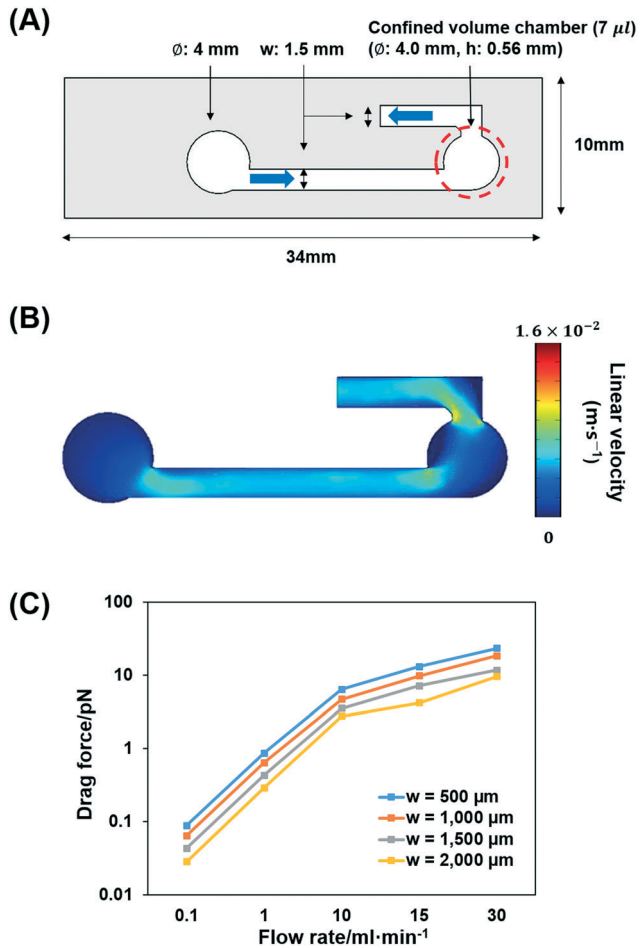

Fig. 3 Numerical analysis of the microfluidic chip. (A) The design of the channel and its dimensions, (B) the linear velocities inside the channel (channel width = 2000 μm, flow rate = 30 ml min^{-1}), and (C) the drag force with various flow rates on the sensing surface.

channel that does not cause C-HRP rupture over a wide range of fluidic flow (from 0.1 to 30 ml min^{-1}). Various widths of the channel (*i.e.*, 500, 1000, 1500, and 2000 μm) in the experiment were considered to investigate the effect of the rupture of immune complexes. The maximum drag force (F_D) of a given velocity was calculated using the following equation:[24]

$$F_D = \frac{1}{2}\rho {v_{max}}^2 C_D A \quad (2)$$

where ρ is the density of the fluid (saliva), v is the velocity of the fluid, C_D is the drag coefficient, and A is the cross-sectional area. For our microfluidic chip, ρ = 1.102 kg m^{-3}, C_D = 0.82, A = 8.792 × 10^{-7} m^2, and v were measured using the COMSOL simulation at a fluid linear velocity of 0.1 μm above the working electrode (Fig. 3B).[25] Additional velocity profiles at different channel widths and flow rates are described in Fig. S1 (ESI†). As illustrated in Fig. 3C, the maximum drag force generated at a flow rate of 30 ml min^{-1}, which is similar to the actual hand injection condition, was greater than the antigen–antibody interaction force under channel widths of 500 μm (23.2 pN) and 1000 μm (18.4 pN). In addition, when the channel width was 2000 μm, the PDMS wall between the channel and the outside became thinner, causing occasional unintentional fluid leakage. Consequently, 1500 μm was selected as the optimal channel width. This condition did not cause any leakage, and the generated drag force (11.6 pN) did not exceed the breaking force.

3.3. Biosensing surface modification for cotinine detection

The bio-recognition layer formation on the sensing surface was characterized using voltammetric and EIS techniques (Fig. 4). EIS is one of the most favorable electrochemical methods and is extensively used in electrochemical biosensing assays. This non-destructive technique is not only used to characterize the sensing surfaces but also applied to monitor the interfacial interactions of biomolecules.[26] As biomolecules are immobilized on the conductive supports, the resistance properties of the electrode–electrolyte change. Based on the molecular and immobilization properties of the sensing interface, the double-layer capacitance diminishes, and the interfacial electron-transfer kinetics decelerate as well.[27] Fig. 4B shows the EIS spectra for different modification steps of SPGE. No semicircle is observed for bare SPGE in the high-frequency region and shows low charge-transfer resistance at the gold electrodes (curve a). The presence of an MPA monolayer on the electrode surface creates negative charges on the surface in neutral pHs (curve b). The electrostatic repulsion between the $[Fe(CN)_6]^{3-/4-}$ redox probe and a negatively charged surface results in an electron transfer resistance equal to 300 Ω. Upon the immobilization of anti-cotinine on the electrode surface, the approach of the redox probe to the surface is more impeded, and the interfacial electron transfer resistance increases by up to 2000 Ω (curve c). A similar trend is obtained upon the immobilization of BSA on the electrode surface and the subsequent interaction of C-HRP with anti-cotinine (2800 and 4500 Ω for curves d and e, respectively). The presence of protein/enzyme molecules on the electrode surface results in the formation of a dielectric impediment to interfacial electron transfer reactions, leading to an enhanced electron transfer resistance. By replacing C-HRP (macromolecule) with cotinine (small molecule), the redox probe can approach the sensing surface more easily and the electron transfer resistance diminishes to 3800 Ω (curve f). Cyclic voltammetry was also used to monitor the modification steps of the electrode surface. Fig. 4C shows the cyclic voltammograms of $[Fe(CN)_6]^{3-}$ on the unmodified and modified SPGE. The negative charges, which developed on the electrode surface owing to MPA self-assembly, result in a reduction in the faradaic peak current (I_p) and an extension in the peak potential separation (ΔE_p) (curve b). Subsequently, the immobilization of anti-cotinine, BSA, and C-HRP on the electrode surface more significantly impedes the access of $[Fe(CN)_6]^{3-}$ to the biosensing surface. Therefore, ΔE_p increases, and I_p decreases more (curves c, d, e). At the final step, C-HRP is replaced with cotinine. As

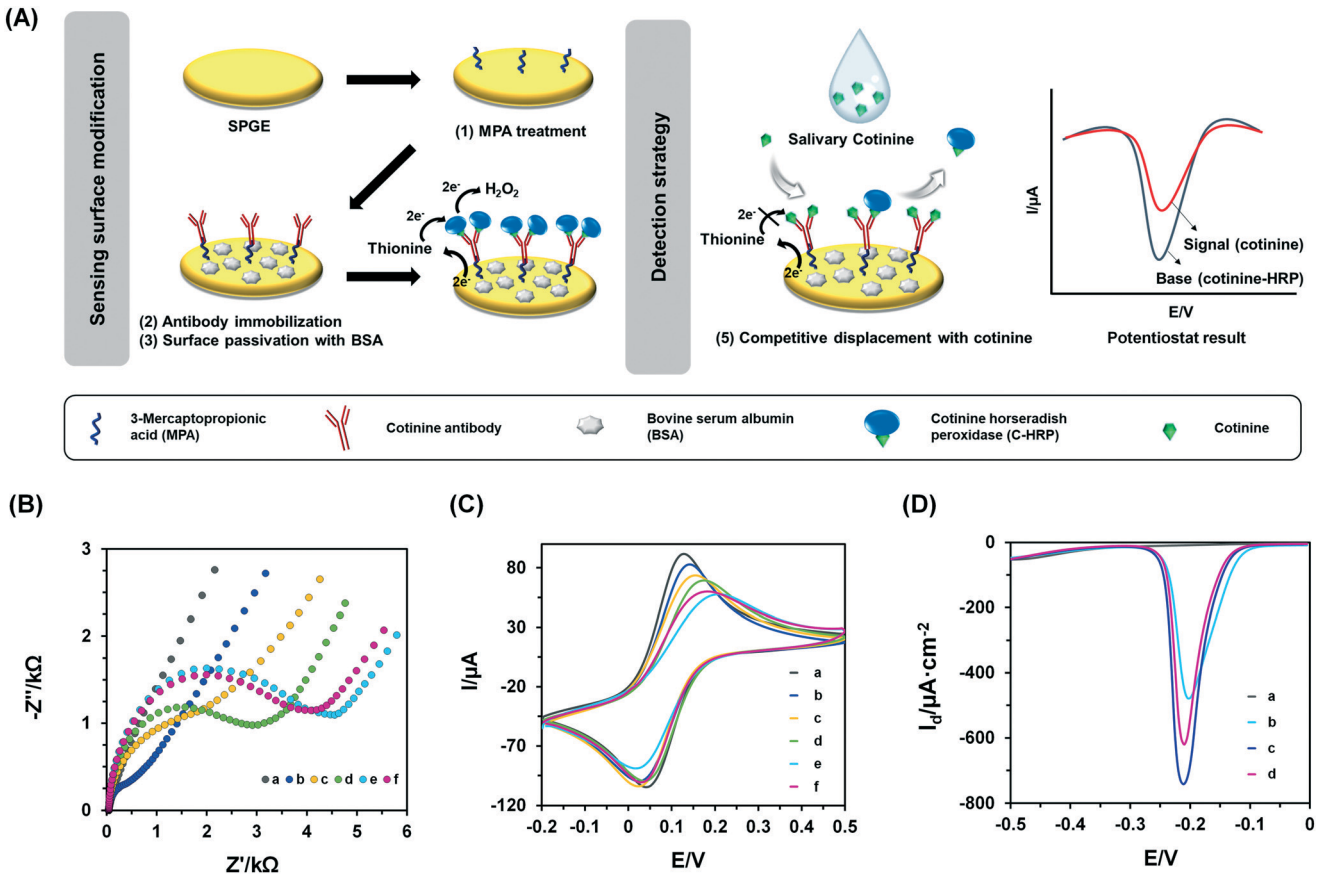

Fig. 4 (A) Schematic representation of the electrochemical immunosensor for cotinine detection. Characterization of different modification steps of the sensing surface by (B) electrochemical impedance spectroscopy in 5×10^{-3} m $[Fe(CN)_6]^{3-/4-}$ (1 : 1) and 0.1 m KCl solution at a constant dc potential of +0.21 V, and (C) cyclic voltammetry in 5×10^{-3} m $[Fe(CN)_6]^{3-}$ and 0.1 m KCl solution at a scan rate of 0.1 V s^{-1} for (a) SPGE, (b) MPA/SPGE, (c) anti-cotinine/MPA/SPGE, (d) BSA/anti-cotinine/MPA/SPGE, (e) C-HRP/BSA/anti-cotinine/MPA/SPGE, and (f) cotinine/C-HRP/BSA/anti-cotinine/MPA/SPGE. (D) Differential pulse voltammograms of C-HRP/BSA/anti-cotinine/MPA/SPGE in (a) dilution solution, (b) dilution solution containing 0.3 μm Thi, and (c) probe solution and cotinine/BSA/anti-cotinine/MPA/SPGE in (d) probe solution.

cotinine is immobilized on the sensing surface, the approachability of negatively charged $[Fe(CN)_6]^{3-}$ ions to the sensing surface becomes easier. Therefore, growth in I_p and contraction in ΔE_p were observed (curve f). The obtained results are in good agreement with the EIS results.

Fig. 4D shows the DPVs of C-HRP/anti-cotinine/SPGE recorded in dilution buffer, in dilution buffer containing Thi, and in probe solution and also the DPV of cotinine/anti-cotinine/SPGE in probe solution. No peaks were observed for the C-HRP/anti-cotinine/SPGE in dilution buffer at 50 mV s^{-1} (curve a) (CVs represented in Fig. S2†). In the presence of dilution buffer containing 0.3 mM Thi, the immunosensor exhibited a pair of clear redox peaks at −0.176 and −0.216 V (curve b), respectively, demonstrating that Thi is the desired electroactive probe and facilitates electron transfer. Afterward, upon the addition of H_2O_2 to the Thi solution, clear catalytic activity appeared with a significant growth in the reduction current density (I_d) and a diminishing of the oxidation current density. In addition, the reduction peak potential shifted moderately in the negative direction (curve c). This behavior demonstrates that captured HRP effectively catalyzes the oxidation of Thi in the presence of H_2O_2 very well.[28] Both captured HRP and Thi mediator should exist in the electrocatalytic reaction cycle. The mechanism of the immunosensor in the Thi/H_2O_2 redox system is outlined as follows:[29]

$$H_2O_2 + HRP_{(red)} \rightarrow H_2O + O_2 + HRP_{(ox)} \quad (3)$$

$$HRP_{(ox)} + Thi \rightarrow HRP_{(red)} + Thi(H)^+ \quad (4)$$

$$Thi(H)^+ + H^+ + 2e^- \rightarrow Thi \quad (5)$$

Finally, curve d shows the I_d of Thi/H_2O_2 after replacing C-HRP with cotinine (target molecule) on the electrode surface. Owing to detachment of C-HRP and the elimination of the enzyme molecule, the reduction current density decreases dramatically. This phenomenon is the basis of the present immunosensor.

3.4. Optimization of detection conditions

This part is shown in the ESI.†

3.5. Analytical performance of the electrochemical immunosensor for cotinine detection

The efficiency of the electrochemical competitive immunosensor for detecting trace amounts of cotinine and its stability, reproducibility, and selectivity were investigated under optimized conditions. To investigate the performance of the electrochemical immunosensor, it was challenged with various concentrations of cotinine on the basis of competitive displacement under optimal conditions. Then, differential pulse voltammograms were recorded in probe solution. As shown in Fig. 5A, the current density decreased with increasing cotinine concentration proportionally. A linear inverse correlation was observed between the Thi reduction current density and the cotinine concentrations. This implies that C-HRP conjugated molecules on the sensor surface were replaced by cotinine molecules. In Fig. 5B, the current density is inversely proportional to the cotinine concentration over the range of 1.0×10^{-1} to 1.0×10^{4} pg ml^{-1}. The limit of detection was calculated as 6×10^{-2} pg ml^{-1} based on three times the standard deviation of the blank (current density achieved when the immunosensor was treated with PBS buffer without cotinine). The limit of quantification was obtained as 1×10^{-1} pg ml^{-1}. Given the obtained results, the significant advantage of the presented immunosensor is its ability to detect cotinine over a wide linear dynamic range with a pico-scale limit of detection. The analytical performance of the introduced immunosensor was compared with previously published methods for the detection of cotinine, as shown in Table S2 (ESI†). Although in the presented platform, the analysis time is longer than some of the other reported methods, the detection limit, linear dynamic range, cost-effectiveness and simplicity of the introduced immunosensor are significantly better than those of previous methods.

The selectivity of the present immunosensor was evaluated by comparing the signal obtained for cotinine (1×10^{2} pg ml^{-1}) and tenfold concentration of cotinine analogs including NIC, TCT, and NN′ with respect to cotinine (1×10^{3} pg ml^{-1}). In addition, assay buffer was used as a blank sample. The small variability between different immunosensors was considered by normalizing changes in the current density ($i_{d0} - i_d$)

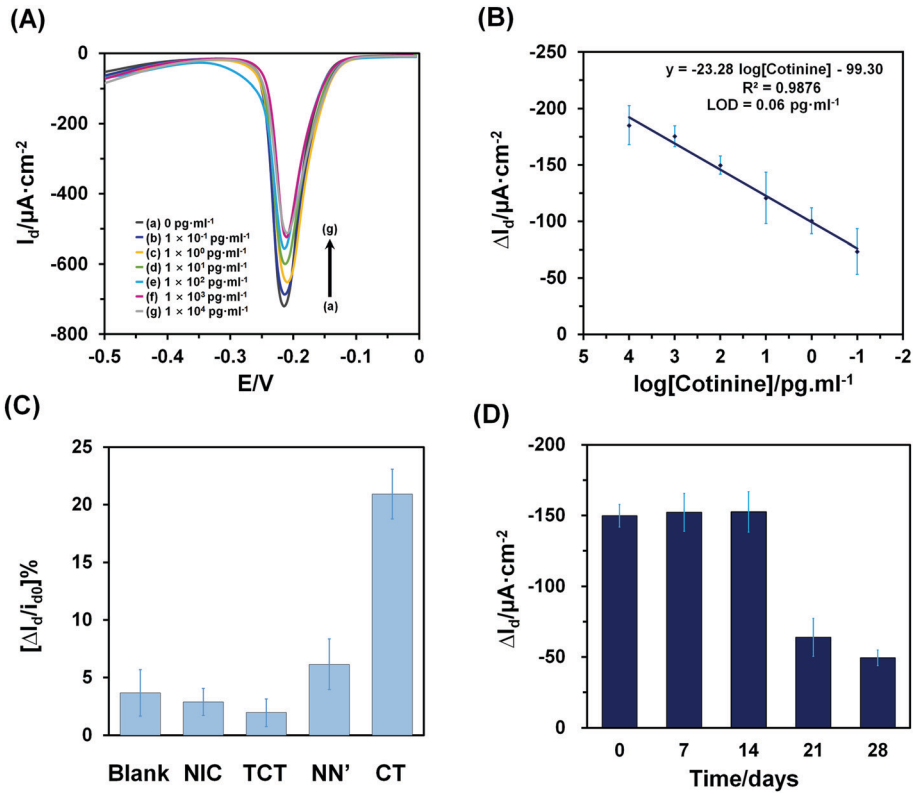

Fig. 5 (A) Differential pulse voltammograms of the C-HRP/BSA/anti-cotinine modified SPGE in the presence of various concentrations of cotinine (a: 0, b: 1×10^{-1}, c: 1×10^{0}, d: 1×10^{1}, e: 1×10^{2}, f: 1×10^{3}, and g: 1×10^{4} pg ml^{-1}) in probe solution. (B) Calibration curve of the immunosensor for cotinine detection; the data points and error bars pertain to the mean and standard deviations of three independent measurements, $\Delta I_d = i_{d0} - i_d$ where i_{d0} is the current density before adding cotinine and i_d is the current density after incubation of the immunosensor with a specified concentration of cotinine, in probe solution. (C) Histograms of normalized current recorded in 1×10^{2} pg ml^{-1} cotinine (CT), 1×10^{3} pg ml^{-1} cotinine homologs including NIC, TCT, and NN′, and blank. Normalized current is $\Delta I_d/i_{d0}$, where $\Delta I_d = (i_{d0} - i_d)$, i_{d0} is the current density before adding cotinine and i_d is the current density after incubation of the immunosensor with a specified concentration of cotinine. (D) Stability test results for the immunosensor stored at 4 °C for 28 days. Data points and error bars are related to the mean and standard deviations of three independent measurements.

with the related i_{d0} values (i_{d0} and i_d definitions have been defined in the caption to Fig. 5). The results indicated that none of the cotinine analogs causes serious interference in cotinine detection. As Fig. 5C shows that even in the presence of tenfold excess of the cotinine concentration, the normalized signal remained almost within 10% of the cotinine signal, which indicates an efficient selective performance of this immunosensor.

The reproducibility of the immunosensor was assessed by the relative standard deviation (RSD) of an intra- and inter-assay. The intra-assay precision of the immunosensor was examined by analyzing three samples in 6 hours. The intra-assay RSD using this biosensor was 4.7% at 1×10^2 pg ml^{-1} cotinine. Likewise, the inter-assay RSD for three immunosensors, 7.4% at 1× reproducibility of the introduced immunosensor, was satisfactory. Last but not the least, the storage stability of the developed immunosensor was assessed. For the stability investigation, C-HRP/anti-cotinine/SPGE was kept in a humid environment at 4 °C for 28 days and applied for the analysis of 1×10^2 pg ml^{-1} cotinine. As Fig. 5D shows, the signal was impressively stable within 14 days. The superior obtained stability and reproducibility are due to a strong bond between anti-cotinine and the gold electrode. This is an important feature for on-site analysis.

3.6. Validation of the all-in-one platform

To prove the applicability of the all-in-one platform, using several collectors and flow rates of injection, the electrochemical signals from C-HRP/BSA/anti-cotinine/MPA/SPGE were measured after delivering the artificial saliva. Here, three cotton-swab-type collectors were used: Salivette, Super•SAL™ and MiriMoa•SAL Collect (Fig. 6A). The collectors were fully soaked in 1 mL of the artificial saliva without cotinine. They were easily assembled into the extraction part of the all-in-one platform and compressed by hand for 2 s to transport bubble-depleted artificial saliva onto the sensing surface. During the loading of the artificial saliva, no leakage was found from the microfluidic chip integrated with the immunosensor. The electrochemical measurements were conducted by DPV under the same conditions described in Fig. 5. The current densities derived from the enzymatic catalysis of C-HRP were analyzed, as shown in Fig. 6B. As a result, regardless of the types of collector, stable catalytic DPV signals were obtained compared with the bare condition in which the artificial saliva was not introduced.

In addition, the effect of the drag force exerted by the injecting pressure on the sensing surface was studied when the saliva was transported at various flow rates. The artificial saliva was delivered at 0.1, 1, and 9 ml min^{-1} by a peristaltic

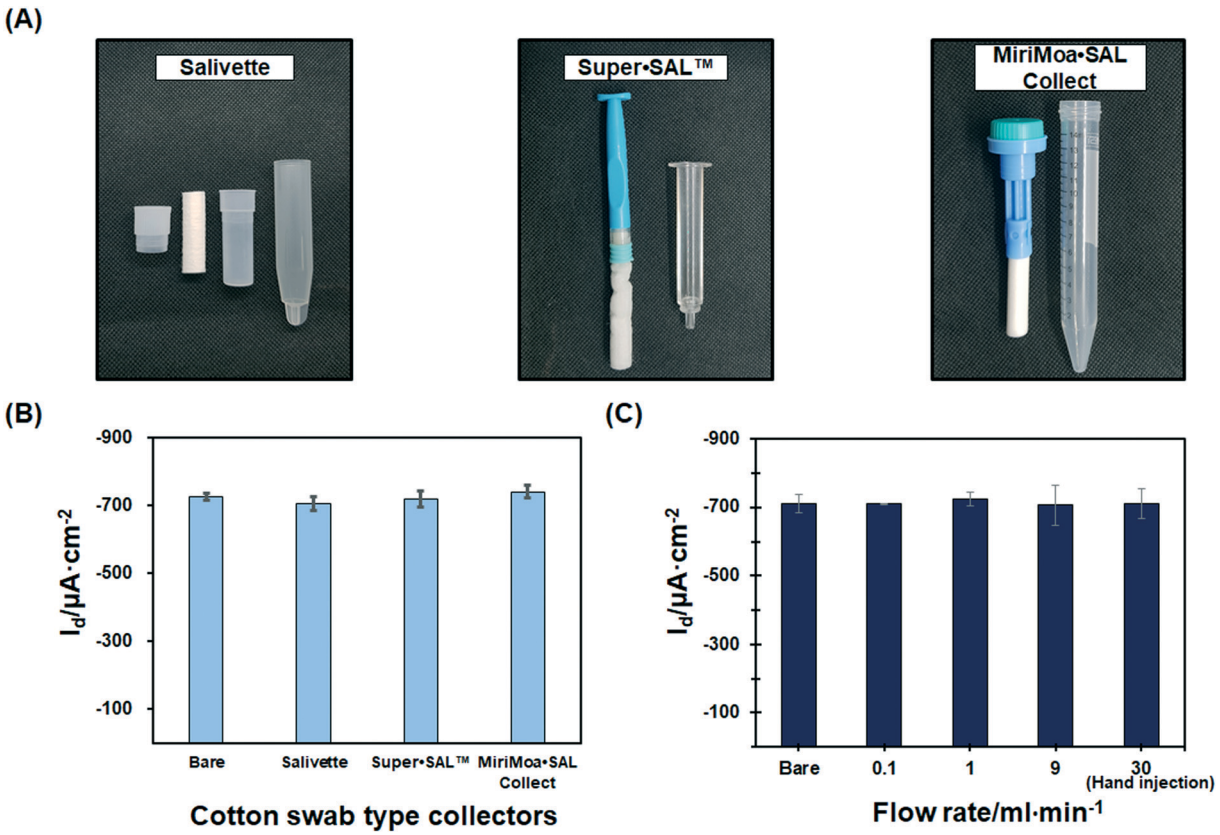

Fig. 6 (A) Commercially available cotton-swab-type collectors, (B) applicability validation of the all-in-one platform with various collectors, and (C) effect of drag force on the sensing surface by saliva injection at various flow rates. Data points and error bars are related to the mean and standard deviations of three independent measurements (in the bare condition, artificial saliva was not introduced).

pump (the available maximum flow rate of the peristaltic pump that we used was 9 ml min^{-1}). Also, direct hand injection was assessed using MiriMoa•SAL Collect. The cotton-swab-type collector, which absorbed 1 mL of the artificial saliva without cotinine, was inserted in the extraction part of the all-in-one platform. To load the artificial saliva onto the sensing surface, the collector was squeezed by hand for 2 s. Under these conditions, the maximum flow rate was calculated as 30 ml min^{-1}. After transferring, the sensing surface (C-HRP/BSA/anti-cotinine/MPA/SPGEs) was examined by monitoring the signal from the enzymatic catalysis of C-HRP by DPV (Fig. 6C). It was observed that no significant changes in the signal occurred in comparison with the response from the bare condition in which the artificial saliva was not introduced. These results suggest that the sensing surface is not affected by the injecting pressure of the saliva with diverse flow rates in the range of 0.1 to 30 ml min^{-1} and show good agreement with the results of the drag force analysis in the microfluidic channels by COMSOL, as described in section 3.2. Therefore, the all-in-one platform has high applicability regardless of the type of commercial collectors and the flow rate for transporting the saliva.

3.7. Application of the all-in-one platform for real human saliva analysis

The saliva tests were performed with two main objectives: to prove the accuracy of the proposed competitive immunosensor and to establish the practicality of the all-in-one platform as a salivary diagnostics tool. To verify the accuracy of the proposed immunosensor, it was applied to analyze the artificial saliva samples spiked with specified quantities of cotinine. The concentration of spiked cotinine was assessed by DPV, and the recorded signals were converted to the concentration of cotinine by a calibration curve equation under the same conditions as those described in Fig. 5. Moreover, the cotinine spiked saliva samples were also evaluated using the LC-MS/MS technique as a standard method. The results acquired with the immunosensor and LC-MS/MS are presented in Fig. 7A. The results showed a great linear correlation between both methods. In addition, for all spiked artificial saliva samples, recovery tests were accomplished by dividing the cotinine concentration found using the immunosensor by the amount added to the artificial saliva samples, as displayed in Table S3.† The recovery values of the immunosensor were in the range of 91% to 107%, demonstrating a high accuracy of the proposed method.

In view of its practicality under realistic conditions, the all-in-one platform was tested with real human saliva. Saliva samples were prepared as described in section 2.5, and the samples were introduced into the cotton swab of MiriMoa•SAL Collect for application to the all-in-one platform. The cotinine level at eight non-smokers' saliva samples was evaluated using DPV under the same conditions as described in Fig. 5. The concentrations of cotinine found using the immunosensor were compared with the results obtained by LC-MS/MS. As shown in Fig. 7B, the range of 45.7 to 890.8 pg ml^{-1} salivary cotinine was measured by the all-in-one platform and the results showed a good correlation with the LC-MS/MS method. In addition, the relative error resulting from the values obtained by the all-in-one platform and the standard method was less than 9.06%, as shown in Table 1. All of the results revealed good consistency with both methods and showed a high practicality of the all-in-one platform as a salivary diagnostic tool.

Based on the questionnaire depicted in Table S1,† saliva samples 1, 2, and 3, which were rarely exposed to second-hand smoke, were found to have 51, 578.8, and 890.8 pg ml^{-1} cotinine, respectively. These results indicated a similar or slightly higher concentration of cotinine than the range of 45.7 to 410.2 pg ml^{-1} found in the saliva of the responders who were exposed to second-hand smoke (sample numbers

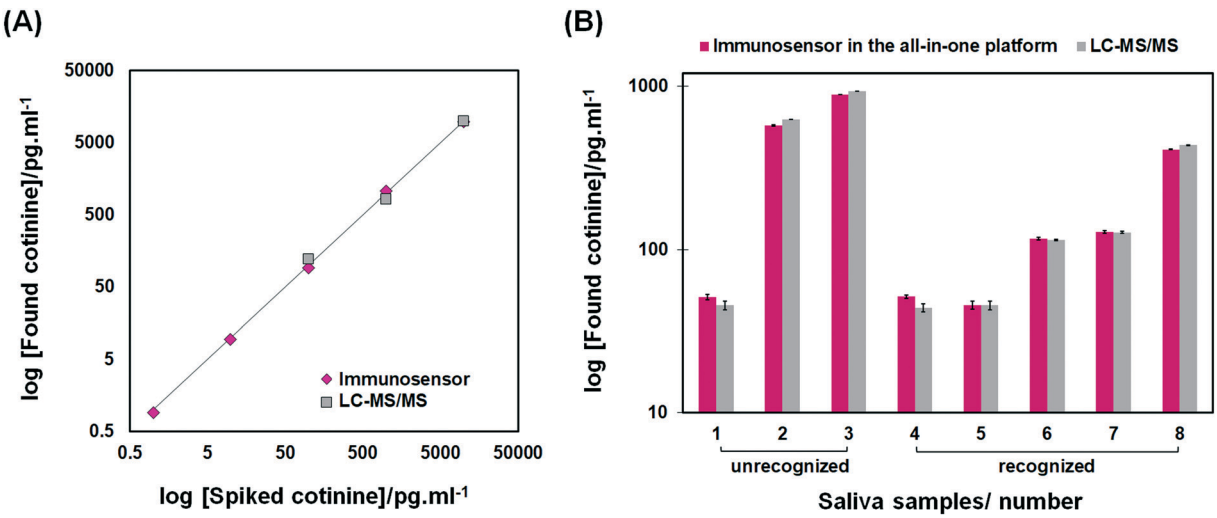

Fig. 7 Salivary cotinine measurement. Determination of cotinine in (A) artificial saliva samples using the electrochemical immunosensor and LC-MS/MS method and (B) real saliva samples from eight volunteers by the all-in-one platform and LC-MS/MS method.

Table 1 Quantitative analysis of cotinine levels in real saliva sample

Saliva samples (number)	Cotinine found by immunosensor (pg ml^{-1})	Cotinine found by LC-MS/MS (pg ml^{-1})	Relative error[a] (%)
1	51 ± 1.9	45.5	9.6
2	578.8 ± 3.3	627.1 ± 0.6	−8.2
3	890.8 ± 3.6	930.8 ± 0.4	−4.3
4	51.3 ± 3.4	44	−2.3
5	45.7 ± 1.2	45.3	0.8
6	116.2 ± 2.7	114.7 ± 0.1	1.3
7	128.4 ± 2.2	127.5	0.7
8	410.2 ± 2.2	435.5 ± 0.1	−5.8

[a] Calculated as [(cotinine found$_{\text{Immunosensor}}$ − cotinine found$_{\text{LC-MS/MS}}$)/(cotinine found$_{\text{LC-MS/MS}}$)] × 100.

4, 5, 6, 7, and 8). This shows the possibility of unrecognized exposure to second-hand smoke[30,31] and signifies the importance of detecting cotinine for a precise analysis of the exposure level to second-hand smoke. Hence, national health care institutions should be aware of this situation and devise countermeasures to protect non-smokers from the unknown threats of exposure to second-hand smoke.

4. Conclusions

We developed an all-in-one platform that assists an electrochemical competitive immunosensor for analyzing salivary cotinine. The all-in-one platform can extract filtered bubble-depleted human saliva from a cotton-swab-type collector and deliver it through a microfluidic chip onto the sensing surface of the immunosensor. A reversible bonding technique using permanent magnets was introduced in the platform to accurately connect and eliminate any leakage between the microfluidic chip and the electrochemical sensor. An in-depth numerical analysis was conducted using computer simulation tools to optimize the pressure from the magnet in the platform and the dimensions of the microfluidic channel.

To the best of our knowledge, this is a new concept of microfluidics integrated electrochemical immunosensor for the detection of salivary cotinine. The established electrochemical immunosensor was based on a competitive binding assay between C-HRP and cotinine to anti-cotinine binding sites. This replacement was monitored electrochemically *via* the catalytic activity of HRP in the presence of a Thi/H_2O_2 redox system. This immunosensor can detect cotinine as low as 6×10^{-2} pg ml^{-1} in a linear dynamic range of 1.0×10^{-1} to 1.0×10^{4} pg ml^{-1}. The presented immunosensor exhibited excellent analytical performance including sensitivity, selectivity, stability, and reproducibility. Furthermore, as a proof-of-concept study, we successfully validated the applicability of the platform and the analysis of cotinine in real human saliva. All of the aforementioned results indicate that the all-in-one platform is a promising device for frequent and on-site monitoring of salivary cotinine and can also contribute to the further development of diverse salivary diagnostic tools. However, despite having all the above-mentioned satisfactory figures of merit, the presented platform has its own limitation. According to some reports the "all-in-one platform" does not cover the entire cutoff values of salivary cotinine related to non-smokers (1.0×10^{4} to 2.5×10^{4} pg ml^{-1}).[32]

Conflicts of interest

There are no conflicts to declare.

Acknowledgements

The authors gratefully thank the National Research Foundation of Korea (NRF) (MSIP) (No. 2015M3A9D7067364, No. 2018R1A2A2A15019814) for their generous financial support to carry out this research.

References

1 US Department of Health and Human Services, *The health consequences of smoking—50 years of progress: a report of the Surgeon General*, USA, 2014.
2 S. S. Hecht, *Nat. Rev. Cancer*, 2003, **3**(10), 733–744.
3 Leading cause of death, illness and impoverishment, http://www.who.int/en/news-room/fact-sheets/detail/tobacco, (accessed 26 July 2019).
4 L. R. Rivero, J. L. Persson, D. C. Romine, J. T. Taylor, T. C. Toole, C. J. Trollman and W. W. Au, *Int. J. Hyg. Environ. Health*, 2006, **209**(1), 1–14.
5 J. S. Pradel, Z. Munshi, A. Jackson, M. Murphy, M. Brown and W. G. Tong, *Proc. SPIE*, 2016, **9948**, 99480E.
6 N. L. Benowitz, K. M. Dains, D. Dempsey, B. Herrera, L. Yu and P. Jacob III, *Nicotine Tob. Res.*, 2009, **11**(8), 954–960.
7 H. Oyama, I. Morita, Y. Kiguchi, E. Banzono, K. Ishii, S. Kubo, W. Yoshiro, H. Anna, K. Chiaki, O. Mitsuhiro and N. Kobayashi, *Anal. Chem.*, 2016, **89**(1), 988–995.
8 Y. Zhang, I. Florath, K. U. Saum and H. Brenner, *Environ. Res.*, 2016, **146**, 395–403.
9 A. N. Ramdzan, M. I. G. Almeida, M. J. McCullough, M. A. Segundo and S. D. Kolev, *TrAC, Trends Anal. Chem.*, 2018, **105**, 89–97.
10 S. Torres, C. Merino, B. Paton, X. Correig and N. Ramírez, *Int. J. Environ. Res. Public Health*, 2018, **15**(12), 2693.
11 J. Shin, S. Chakravarty, W. Choi, K. Lee, D. Han, H. Hwang, J. Choi and H. I. Jung, *Analyst*, 2018, **143**(7), 1515–1525.
12 S. Chojnowska, T. Baran, I. Wilińska, P. Sienicka, I. Cabaj-Wiater and M. Knaś, *Adv. Med. Sci.*, 2018, **63**(1), 185–191.
13 M. Raja, A. Garg, P. Yadav, K. Jha and S. Handa, *J. Clin. Diagn. Res.*, 2016, **10**(3), ZE04.
14 J. M. Yoshizawa, C. A. Schafer, J. J. Schafer, J. J. Farrell, B. J. Paster and D. T. Wong, *Clin. Microbiol. Rev.*, 2013, **26**(4), 781–791.
15 I. H. Valdez and P. C. Fox, *Crit. Rev. Oral Biol. Med.*, 1993, **4**(3), 271–277.
16 K. A. Hyun, H. Gwak, J. Lee, B. Kwak and H. I. Jung, *Micromachines*, 2018, **9**(7), 340.
17 R. S. Malon, S. Sadir, M. Balakrishnan and E. P. Córcoles, *BioMed Res. Int.*, 2014, 2014.

18 M. S. Khan, K. Dighe, Z. Wang, I. Srivastava, E. Daza, A. S. Schwartz-Dual, J. Ghannam, S. K. Misra and D. Pan, *Analyst*, 2018, **143**(5), 1094–1103.
19 K. Y. Priya and K. M. Prathibha, *Int. J. Dent. Oral Health*, 2017, **3**(3), 149–153.
20 K. P. R. Nilsson and O. Inganäs, *Nat. Mater.*, 2003, **2**(6), 419.
21 J. P. Hoare, *J. Electrochem. Soc.*, 1984, **131**(8), 1808–1815.
22 F. P. Incropera, A. S. Lavine, T. L. Bergman and D. P. DeWitt, *Fundamentals of heat and mass transfer*, Wiley, USA, 1996, vol. 4.
23 U. Dammer, M. Hegner, D. Anselmetti, P. Wagner, M. Dreier, W. Huber and H. J. Güntherodt, *Biophys. J.*, 1996, **70**(5), 2437–2441.
24 G. Falkovich, *Fluid mechanics: A short course for physicists*, Cambridge University Press, UK, 2013.
25 E. L. Boulpaep, W. F. Boron, M. J. Caplan, L. Cantley, P. Igarashi, P. S. Aronson and E. Moczydlowski, *Medical physiology a cellular and molecular approach*, Elsevier Health Sciences, UK, 2009, pp. 48–75.
26 E. Katz and I. Willner, *Electroanalysis*, 2003, **15**(11), 913–947.
27 D. Wild, *The immunoassay handbook: theory and applications of ligand binding, ELISA and related techniques*, Newnes, UK, 2013.
28 C. Ruan, F. Yang, C. Lei and J. Deng, *Anal. Chem.*, 1998, **70**(9), 1721–1725.
29 S. Liu and A. Chen, *Langmuir*, 2005, **21**(18), 8409–8413.
30 R. M. Flores, B. Liu and E. Taioli, *Carcinogenesis*, 2016, **37**(11), 1062–1069.
31 A. Florescu, R. Ferrence, T. Einarson, P. Selby, O. Soldin and G. Koren, *Ther. Drug Monit.*, 2009, **31**(1), 14.
32 S. Kim, *Int. J. Environ. Res. Public Health*, 2016, **13**(12), 1236.

